R-559-PR

November 1970

A PANORAMIC VIEW OF IONOSPHERIC REFLECTION AND TRANSMISSION UNDER AMBIENT AND DISTURBED CONDITIONS

H. G. Booker, C. M. Crain and E. C. Field

A Report prepared for

UNITED STATES AIR FORCE PROJECT RAND

Rand

SANTA MONICA, CA. 90406

This research is supported by the United States Air Force under Project Rand—Contract No. F44620-67-C-0045—Monitored by the Directorate of Operational Requirements and Development Plans, Deputy Chief of Staff, Research and Development, Hq USAF. Views or conclusions contained in this study should not be interpreted as representing the official opinion or policy of Rand or of the United States Air Force.

R-559-PR

November 1970

A PANORAMIC VIEW OF IONOSPHERIC REFLECTION AND TRANSMISSION UNDER AMBIENT AND DISTURBED CONDITIONS

H. G. Booker, C. M. Crain and E. C. Field

A Report prepared for

UNITED STATES AIR FORCE PROJECT RAND

Rand

SANTA MONICA, CA. 90406

Rand maintains a number of special subject bibliographies containing abstracts of Rand publications in fields of wide current interest. The following bibliographies are available upon request:

Africa • Arms Control • Civil Defense • Combinatorics
Communication Satellites • Communication Systems • Communist China
Computing Technology • Decisionmaking • Delphi • East-West Trade
Education • Foreign Aid • Foreign Policy Issues • Game Theory
Health-related Research • Latin America • Linguistics • Maintenance
Mathematical Modeling of Physiological Processes • Middle East
Policy Sciences • Pollution • Program Budgeting
SIMSCRIPT and Its Applications • Southeast Asia • Systems Analysis
Television • Transportation • Urban Problems • USSR/East Europe
Water Resources • Weapon Systems Acquisition
Weather Forecasting and Control

To obtain copies of these bibliographies, and to receive information on how to obtain copies of individual publications, write to: Communications Department, Rand, 1700 Main Street, Santa Monica, California 90406.

Published by The Rand Corporation

PREFACE

This report is part of Rand's continuing study of the effects of abnormally ionized atmospheres, such as those produced by nuclear bursts, on the propagation of radio waves and on military radio communication systems, present and future. As a tool useful for providing answers to many problems arising in such studies, we have developed a general computer program which could be applied over a wide range of frequencies (typically 10^{-3} to 10^{10} Hz) for any specified vertical ionization structure of the atmosphere. Both electrons and positive and negative ions are included in the program. For specified frequencies, angle of wave incidence on the ionosphere, and ionization profiles the program provides the real and imaginary components of the complex refractive index at all heights, the local wavelength of the signal, the differential absorption at all heights, and the reflection and transmission parameters for the nonpenetrating and penetrating signal components, respectively. The program provides results for either quasi-longitudinal or quasi-transverse conditions of transmission.

The program is developed from a ray theory approach and as such has certain restrictions and accuracy limitations, in particular at the lower frequencies used. Despite such limitations the program is a very versatile tool for obtaining results which can be applied to practical assessment of many problems in radio transmission, both for earth-to-earth and earth-to-space radio links, and for ambient or arbitrarily disturbed ionospheres.

Selected results obtained from the program are presented in this and a companion report, R-558-PR, *Transmission of Electromagnetic Waves Through Normal and Disturbed Atmospheres.*

Henry G. Booker is Chairman of the Department of Applied Physics and Information Science at the University of California, San Diego and is a consultant to The Rand Corporation.

SUMMARY

This report presents the technical basis used in the development of a computer program for assessing the effects of ambient and disturbed daytime and nighttime ionospheres on the reflection and transmission of radio waves in the 10^{10} to 10^{-3} Hz frequency range. The ionospheric models and electromagnetic theory used are described, certain limitations are discussed, and the parameters and equations used are summarized. A number of results obtained from the program are presented in graphical form. From these, the existence of height-dependent pass bands, stop bands, and conduction bands in the ionosphere is evident. Also shown are reflection levels and two-way reflection losses. These results provide useful understanding of ionospheric wave propagation, and serve as background material. Results with direct engineering application to earth-satellite communication links have also been obtained, and are given in a companion report.

CONTENTS

I. INTRODUCTION

In this report a technical description of a computer program we have developed is given, along with some diagrams which present a useful overall impression of the effects of the ionosphere on both reflection and transmission over the entire range of frequencies from microwave to hydromagnetic (10^{10} to 10^{-3} Hz). Ambient day and night conditions are treated, as well as disturbed conditions corresponding either to a mild nuclear environment or a severe polar cap absorption (PCA) event. In addition to the material included in this report, which is useful for purposes of general interpretation and understanding of propagation characteristics, we have obtained results with direct engineering applicability to satellite-earth communication links. These are presented in a companion report[1] in the form of coefficients of transmission through the ionosphere and height profiles of attenuation.

Section II describes the assumptions made and the models used, and Section III gives the numerical results and related discussion. The Appendix details the wave-propagation equations and the parameters used in the computer program from which the results of the report were derived. The wave equations are those of the magneto-ionic theory, taking both electrons and ions into account.

II. MODEL AND ASSUMPTIONS

Models of the ionosphere are required that specify as functions of height the electronic and ionic collisional frequencies, the electron density, and the densities of positive and negative ions. Different models are needed for night and day. Also of interest are conditions in which the D region of the ionosphere is disturbed by natural or man-made phenomena. The four profiles of electron and negative ion density used in this study are shown in Fig. 1 and are identified as ambient night, ambient day, disturbed night, and disturbed day.

The ambient profiles of Fig. 1 are typical of those in current use. Positive ion profiles were chosen to maintain charge neutrality. The collisional frequencies used are based on Ref. 2. The principal uncertainty in the profiles involves the distributions of electron density below a value of about 10^8 electrons per cubic meter, where measurements are the most uncertain. The profiles for the disturbed day and night cases are based on electron production rates due to widespread high-altitude fission debris as described in Ref. 3, using a value of 5000 for P_M^*, and nominal reaction rates such as given in Ref. 4. Use of production and reaction rates as recently given in Ref. 5 would be expected to lead to better prediction of the electron and ion distributions; however, the differences are small and not significant for the purposes of this report. Although the disturbed ionization profiles are representative of a mild nuclear environment from high-altitude fission debris, the values of electron and ion density in the important height region from about 40 to 80 km are approximately those expected for a severe polar-cap disturbance, and hence the transmission and reflection results can be taken to be appropriate for such a disturbance. The ambient and disturbed cases thus represent the approximate lower and upper limits of naturally occurring ionospheric structures.

The major approximation is the use of WKB methods to compute the transmission and reflection losses. This, of course, neglects the

---

*$P_M = 5 \times 10^{13} \dfrac{\text{fission yield in megatons}}{(\text{debris radius in km})^2 \, t_{\text{sec}}^{1.2}}$

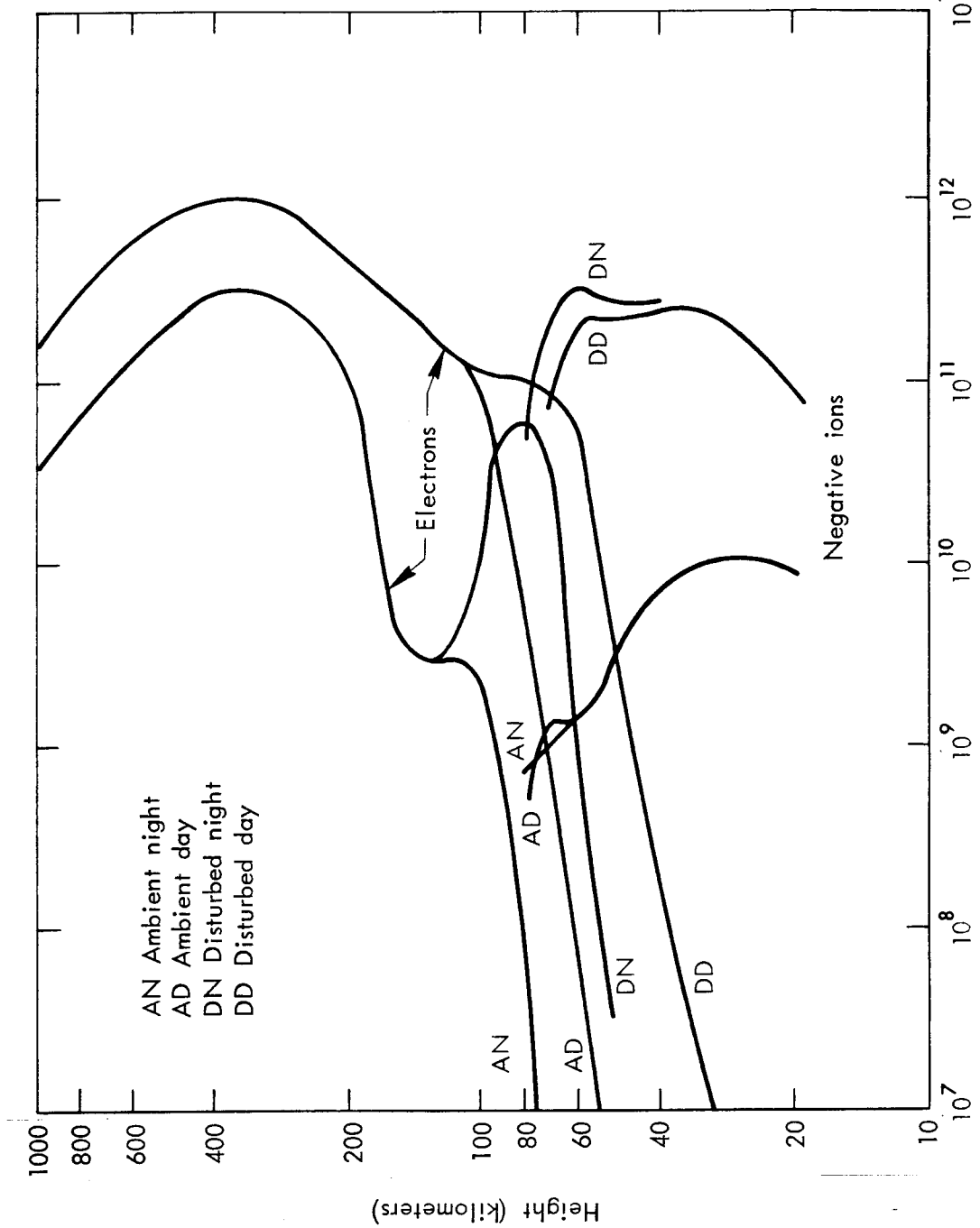

Fig. 1—Ionospheric models for the ambient night, ambient day, disturbed night, and disturbed day ionospheres

effects of gradient reflection and is valid provided that the wavelength *in the ionosphere* is smaller than the characteristic distance over which the ionospheric refractive index changes substantially--typically a few kilometers. In Fig. 2 we show the ratio of the wavelength in the ionosphere to the free-space wavelength as a function of height for a range of frequencies and ambient day and night conditions. The ratios were computed from the equations given in the Appendix. Note that the wavelength is shortened considerably in the ionosphere, especially at the lower frequencies. By multiplying the curves of Fig. 2 by the appropriate free-space wavelength to get the height-dependent absolute wavelength, it can be seen that the WKB solutions should be quite good for frequencies above about 1 kHz. Below about 100 Hz the WKB validity condition is seriously violated. Thus, at frequencies of the order of 100 Hz or less, gradient reflection is not negligible and our results for attenuation correspond to lower bounds on the transmission losses. Similarly, resonances in the transmission coefficients and Brewster's angle effects in reflection coefficients cannot be correctly predicted by WKB methods at these low frequencies. We have spot checked some of the results at frequencies of the order of 1 Hz by using a full-wave numerical method developed by Rand for the study of the ionospheric transmission of geomagnetic micropulsations.[6] In cases where meaningful comparisons could be made, the agreement was within an order of magnitude. This indicates that even at micropulsation frequencies the WKB methods yield useful, albeit rough, estimates. Our conclusion that the WKB methods should be very reliable at frequencies above 1 kHz is confirmed by the work of Jones,[7] who compared full-wave and WKB calculations of ionospheric reflection of waves in the 1 kHz to 10 MHz band. In no case were the WKB calculations in error by more than a few decibels.

The calculations have been performed for the two cases of waves having phase velocities in the vertical direction and at an angle, i, of 80 deg with respect to the vertical at the base of the ionosphere. The geomagnetic field was assumed vertical. Thus, strictly speaking, the results for an incidence angle, i, of zero deg correspond to vertical propagation at a magnetic pole, i.e., vertical longitudinal

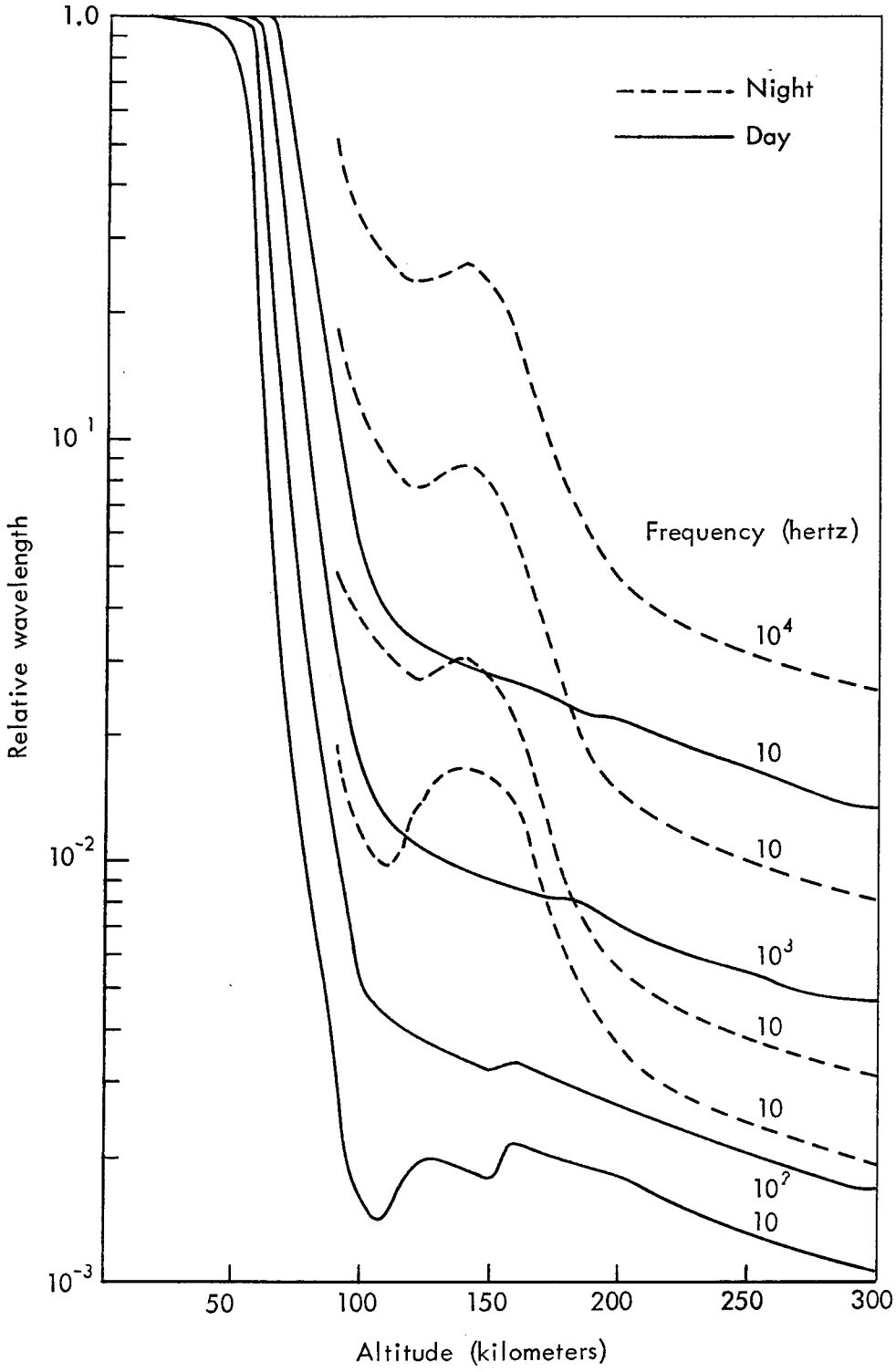

Fig. 2—Local wavelength in medium relative to free-space wavelength (X wave, ambient ionosphere model)

propagation. Booker and Dyce[8] have investigated the range of validity of the quasi-longitudinal (QL) approximation for hydromagnetic waves and radio waves in the ionosphere and magnetosphere in the absence of collisions. We have here re-examined the validity range after including collisions, which increase the accuracy of the QL approximation, and for vertical propagation the conclusions are these:

1. At altitudes above about 150 km, where electron-neutral and ion-neutral collisions tend to be relatively unimportant, the QL approximation is valid for geomagnetic dip angles larger than 40 deg if the wave frequency exceeds about 10 Hz. For wave frequencies less than about 1 Hz, the QL approximation applies only near the magnetic pole.
2. At an altitude of 120 km, where ion-neutral collisions are important, the QL approximation is valid for dip angles larger than 40 deg for essentially all frequencies considered here.
3. At altitudes below about 70 km, where electron-neutral collisions dominate, the QL approximation is valid everywhere.

Note that at the altitudes where the most important absorption occurs (below 150 km), the QL approximation applies down to mid-latitudes or lower. A detailed application of the QL approximation would involve recalculating the results to be shown using the equations of the Appendix, but at each latitude substituting the vertical component of the geomagnetic field for the total field which now appears in the formulas. This has been done in some cases as a check and, for latitudes above about 40 deg, the losses were only somewhat larger than those obtained from the vertical polar calculations, the results of which are presented in Section III.

At frequencies less than the electronic gyrofrequency, the direction of group propagation (the ray) can differ drastically from the direction of phase propagation (the wave normal) even within the domain of validity of the QL approximation. (See Ref. 8 for a detailed analysis of this phenomenon in the absence of collisional effects.) At VLF frequencies and lower, the ionospheric refractive index is large, and a wave traveling downward from, say, a satellite will have its wave

normal bent strongly away from the vertical upon emergence from the ionosphere. (Actually this occurs over a height range in the lower ionosphere.) Conversely, a low-frequency wave incident obliquely upon the ionosphere from below will have its wave normal bent to nearly the vertical direction within a few ionospheric conductivity-scale heights. In order to emerge, rather than be internally reflected, a downward propagating low-frequency wave must have its normal very nearly vertical while in all but the lowest regions of the ionosphere. Thus our results given here and in Ref. 1, which correspond to vertical or nearly vertical *phase* propagation *in the ionosphere*, apply to realistic satellite-ground phase paths. This is true even though the group path tends to be more or less along the geomagnetic field in the absence of collisions[8] and, for temperate latitudes, can be distinctly non-vertical. The relation between ray and phase propagation direction is not well understood when both collisional and geomagnetic effects are of consequence. In any event, however, the transmission loss is obtained by a vertical or nearly vertical integration over all but the lowest ionospheric heights and our results should in most cases provide reasonable estimates.

As indicated earlier, results also will be given for glancing incidence (or emergence), i = 80 deg. However, the longitudinal assumption is retained for the glancing-incidence calculations. Thus the curves to be shown for glancing incidence give only an indication of where angle of incidence matters and of roughly how much. Recalling that a typical phase path from a VLF/ELF satellite transmitter will be nearly vertical until the lower ionosphere is reached, whence the propagation vector is bent to nearly horizontal, it is evident that for certain satellite - ground-station geometries a portion of the phase propagation path could be nearly perpendicular to the geomagnetic field, even at high latitudes. For such paths, a full analysis involving neither QL nor QT approximations is needed. Such aspects are beyond the scope of the treatment given in this report. It is worth mentioning, however, that we have performed computations for the case where phase propagation is transverse to the geomagnetic field. We will not

present detailed graphs of these results here but will simply point out that the attenuation for transverse propagation was found to be larger than for longitudinal propagation if all other variables are held constant. This indicates that if the QL approximation is violated over part of a phase path, the attenuation and transmission losses will be larger than given here or in Ref. 1.

Finally, note that the effects of earth curvature are neglected.

III. RESULTS AND DISCUSSION

Figures 3 to 10 show frequency plotted horizontally from 10^{-3} to 10^{10} Hz. They show ionospheric height plotted vertically, with heights above 180 km omitted, since it is reasonably obvious what happens beyond that point. Significant frequencies in the figures are the following:

1. The superior penetration frequencies, or "critical frequencies," f_{OF} and f_{XF} of the F region of the ionosphere for the O and X waves (that is, for left-handed and right-handed polarization about the earth's magnetic field, respectively).
2. The electronic gyrofrequency f_{Me}.
3. The ionic gyrofrequency f_{Mi}, separated into an atomic value f_{Ma} above 150 km and a molecular value f_{Mm} below 160 km, with an overlap of atoms and molecules between these two heights. (In the model positive ions were considered molecular below 150 km and atomic above 160 km. The negative ion density above 90 km was assumed zero.)

Figures 3 to 6 refer to night models and Figs. 7 to 10 to day models. Alternate figures refer to the O and X waves. Figures 3 and 4 refer to ambient (undisturbed) conditions at night), while Figs. 7 and 8 refer to ambient conditions in the daytime.

In each diagram is shown the curve for which

$$\nu_e = |\omega_{Me} \pm \omega| \tag{1}$$

where ν_e is the electronic collisional frequency, ω_{Me} is the angular electronic gyrofrequency, ω is the angular wave frequency, and the upper and lower signs refer to the O and X waves, respectively. At heights above this curve the effect of electronic collisions is relatively secondary. Below the level where $\nu_e = \omega_{Me}$ (between 70 and 80 km) the effect of the earth's magnetic field is unimportant. At an altitude between 110 and 120 km the level for which $\nu_i = \omega_{Mi}$ can also be seen, where ν_i is the ionic collisional frequency and ω_{Mi} is the ionic gyrofrequency. Above this level both ionic and electronic collisions

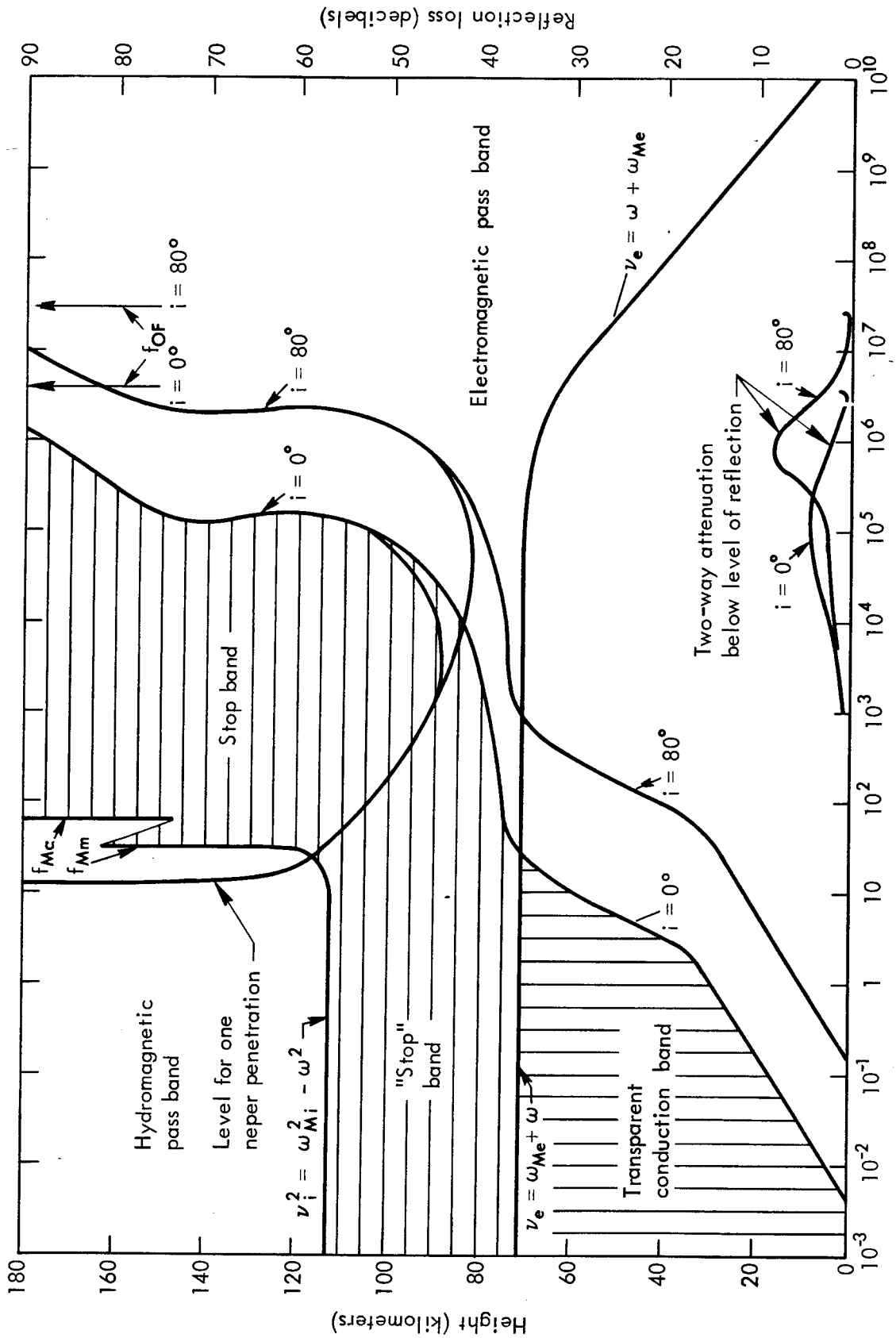

Fig. 3—Quasi-longitudinal propagation of the O wave for ambient (undisturbed) night conditions

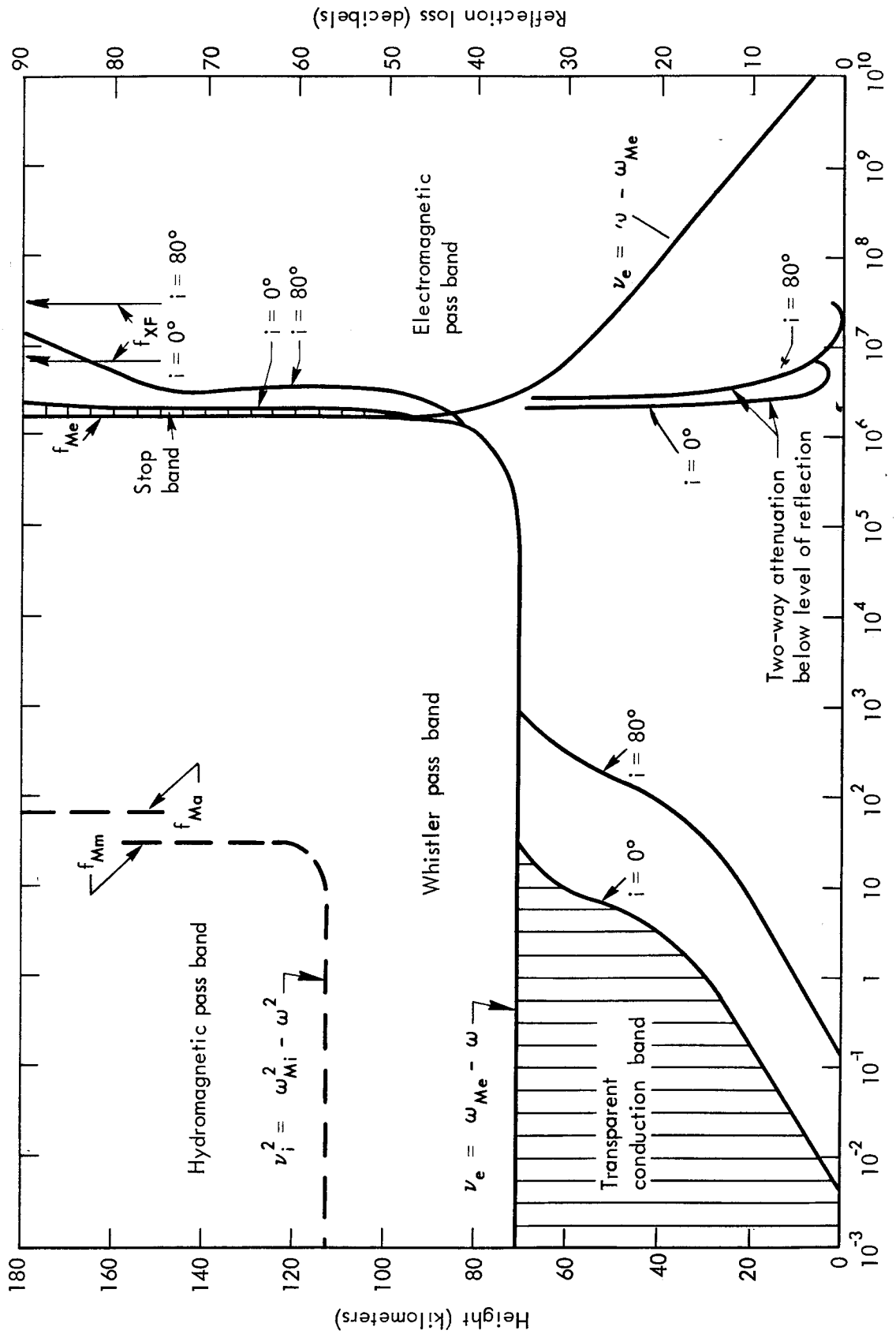

Fig. 4—Quasi-longitudinal propagation of the X wave for ambient (undisturbed) night conditions

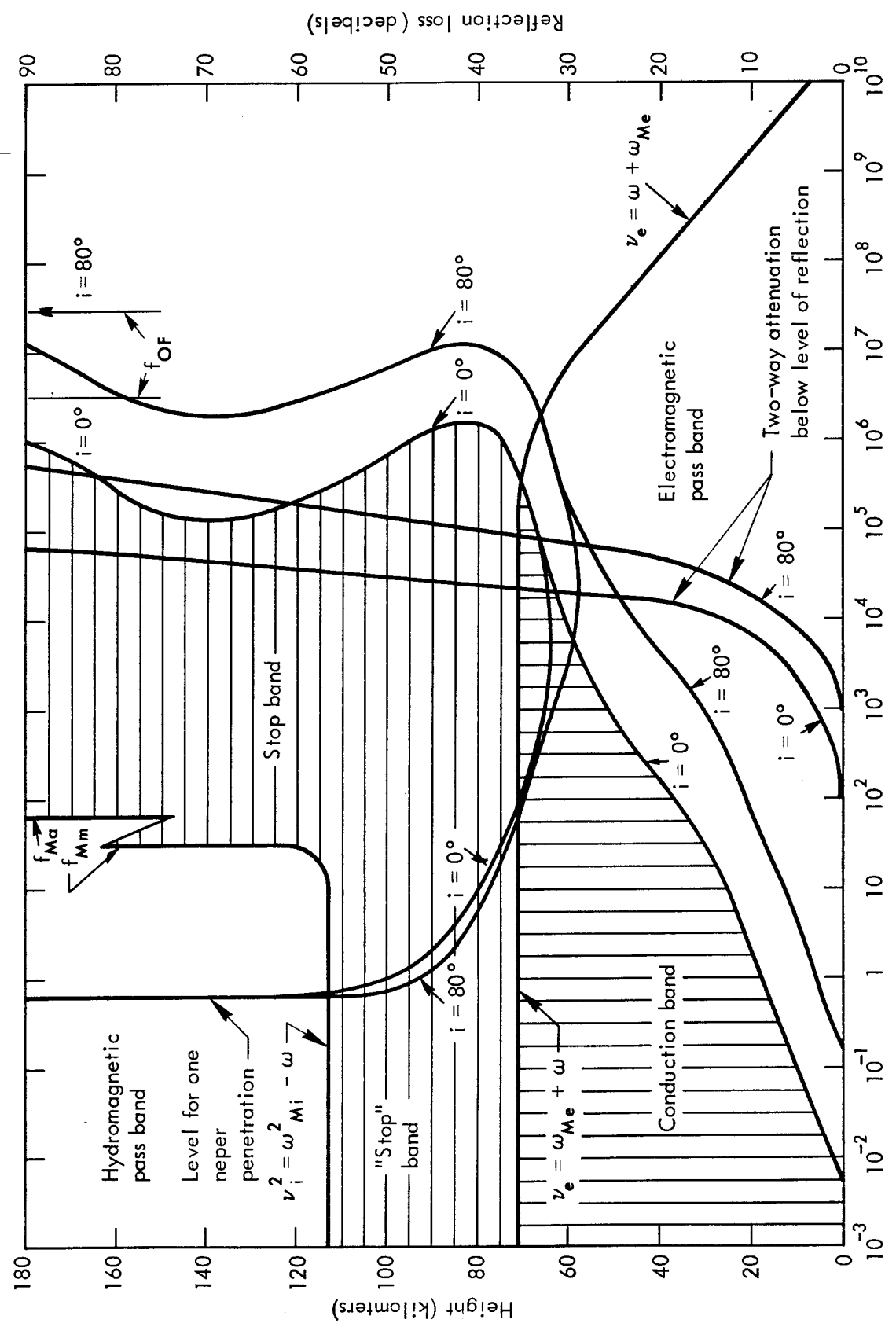

Fig. 5—Quasi-longitudinal propagation of the O wave for disturbed night conditions

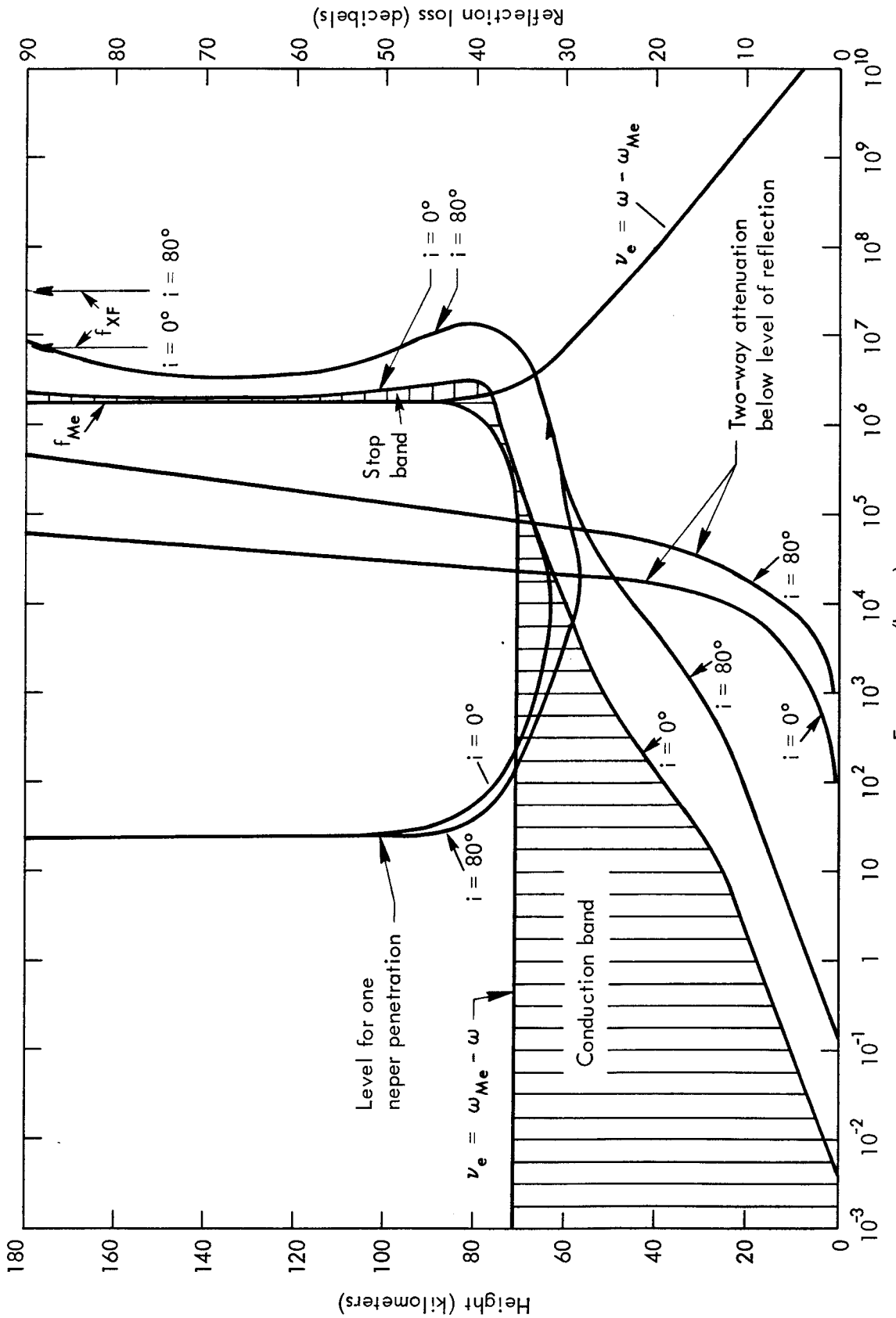

Fig. 6—Quasi-longitudinal propagation of the X wave for disturbed night conditions

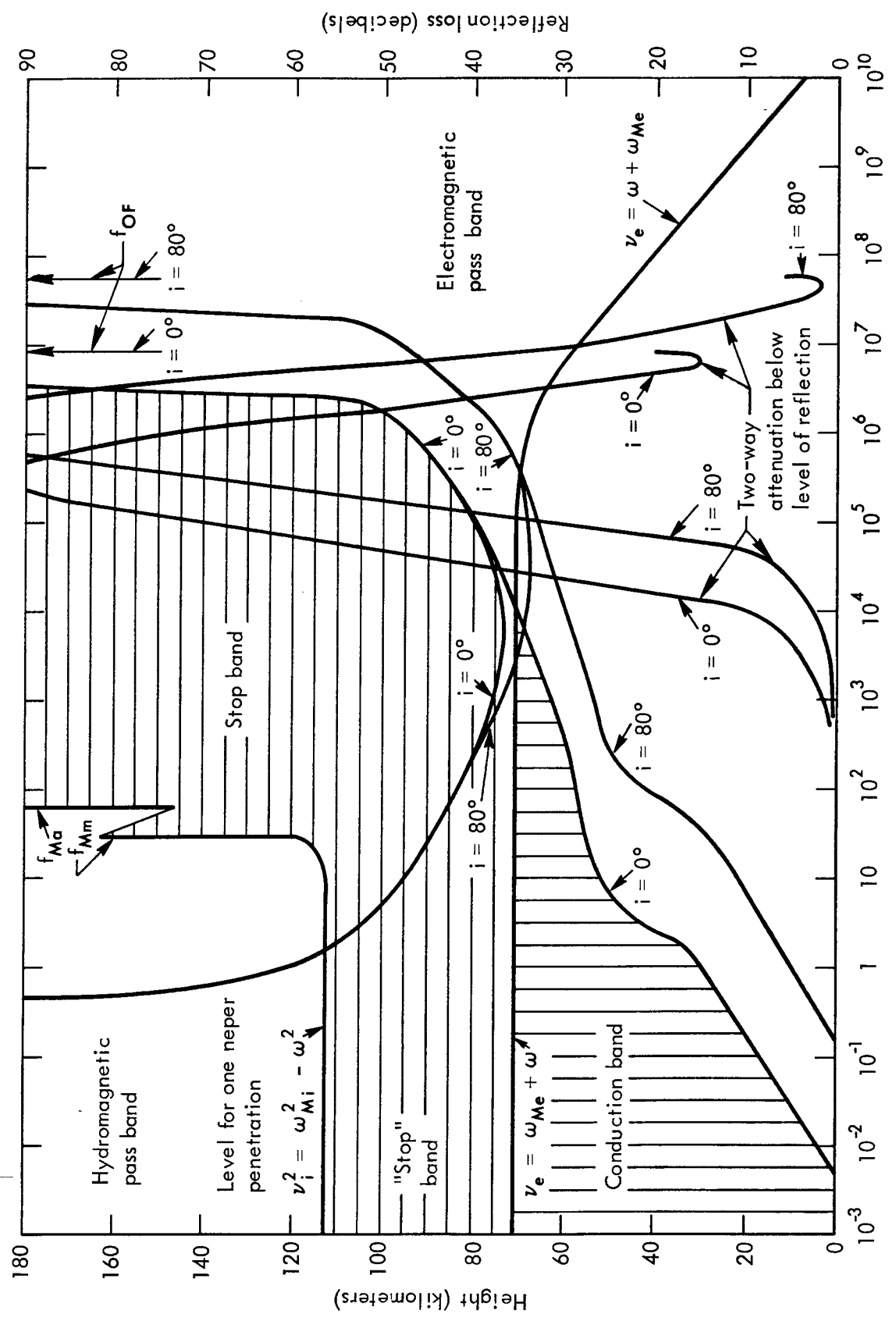

Fig. 7—Quasi-longitudinal propagation of the O wave for ambient (undisturbed) day conditions

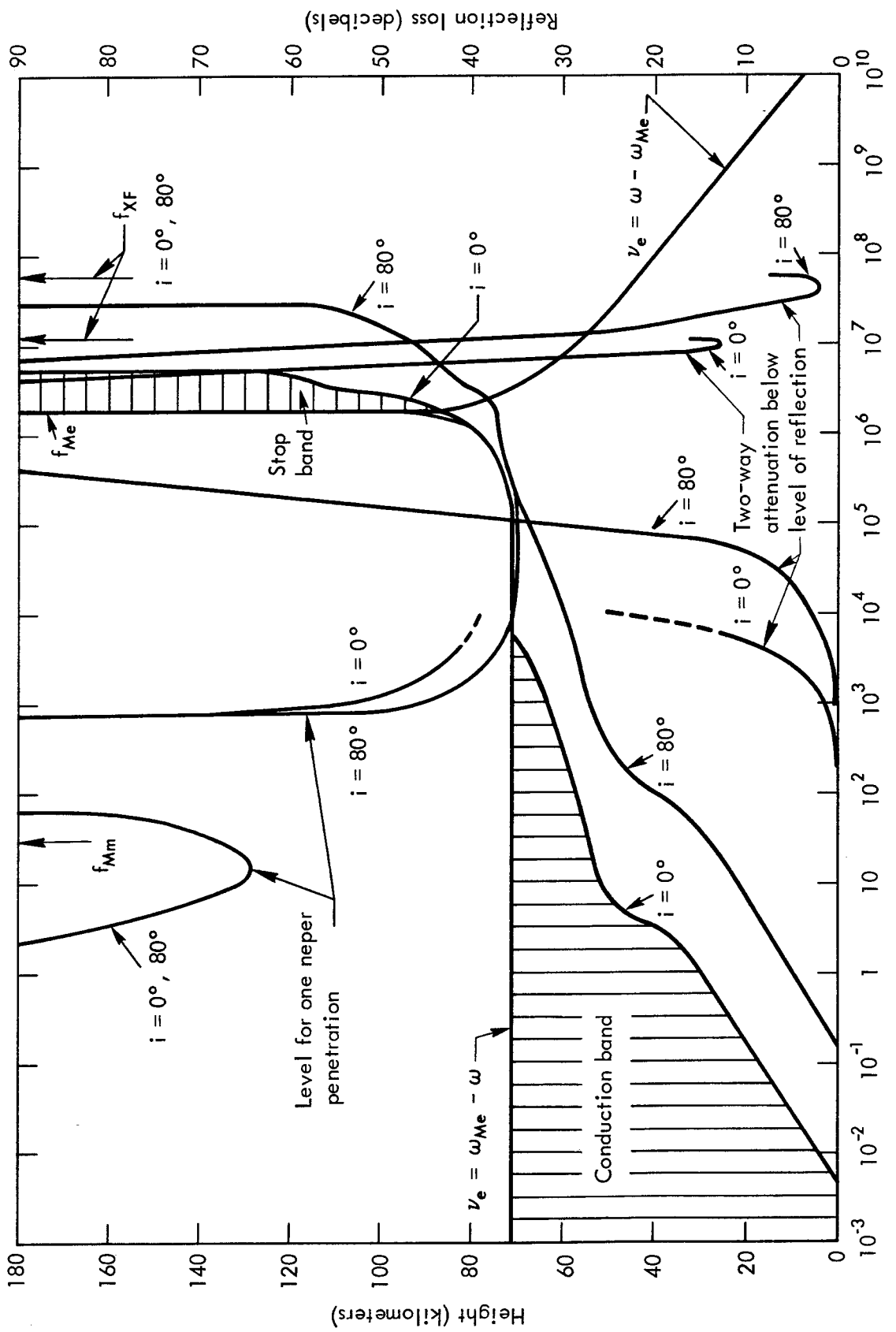

Fig. 8—Quasi-longitudinal propagation of the X wave for ambient (undisturbed) day conditions

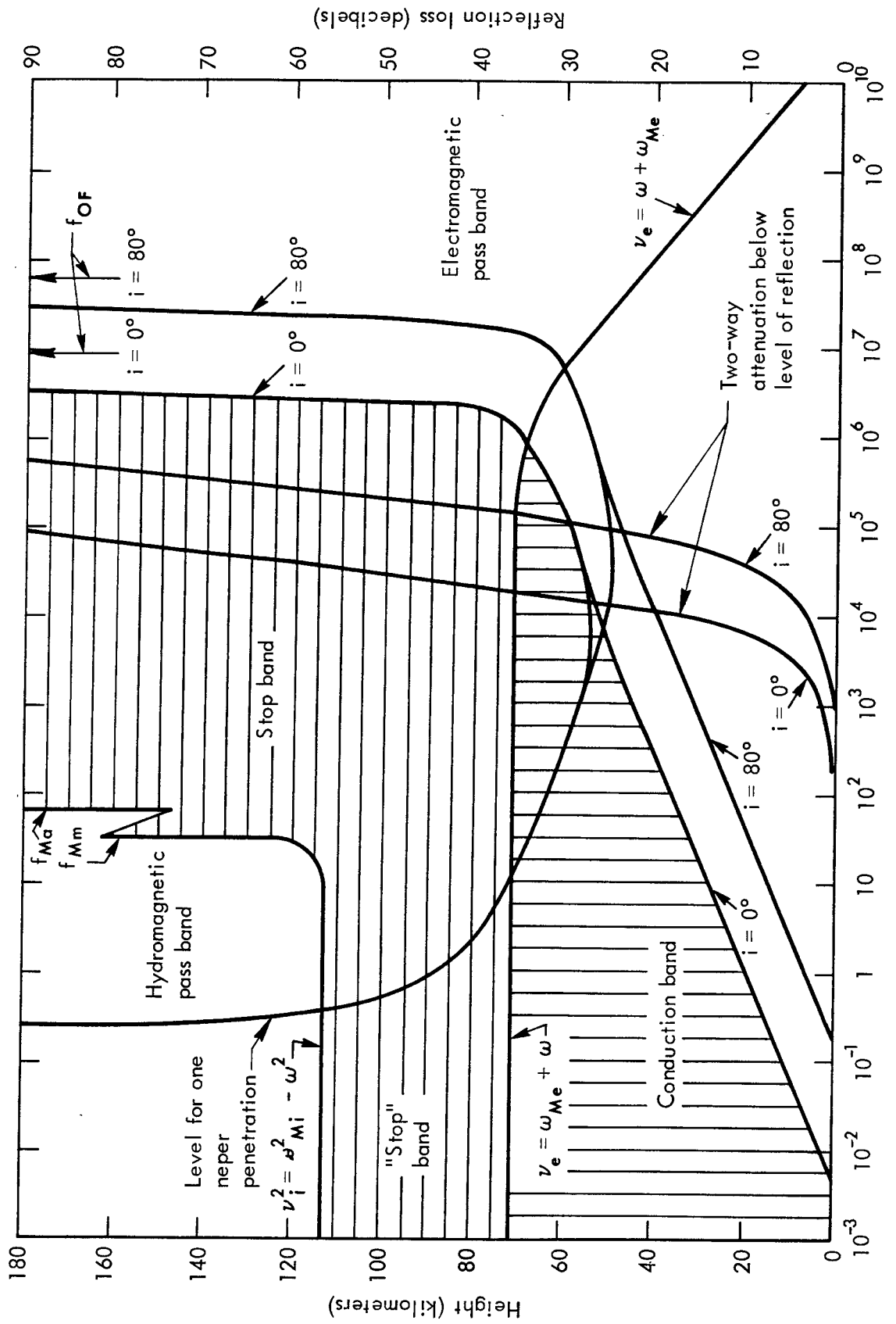

Fig. 9—Quasi-longitudinal propagation of the O wave for disturbed day conditions

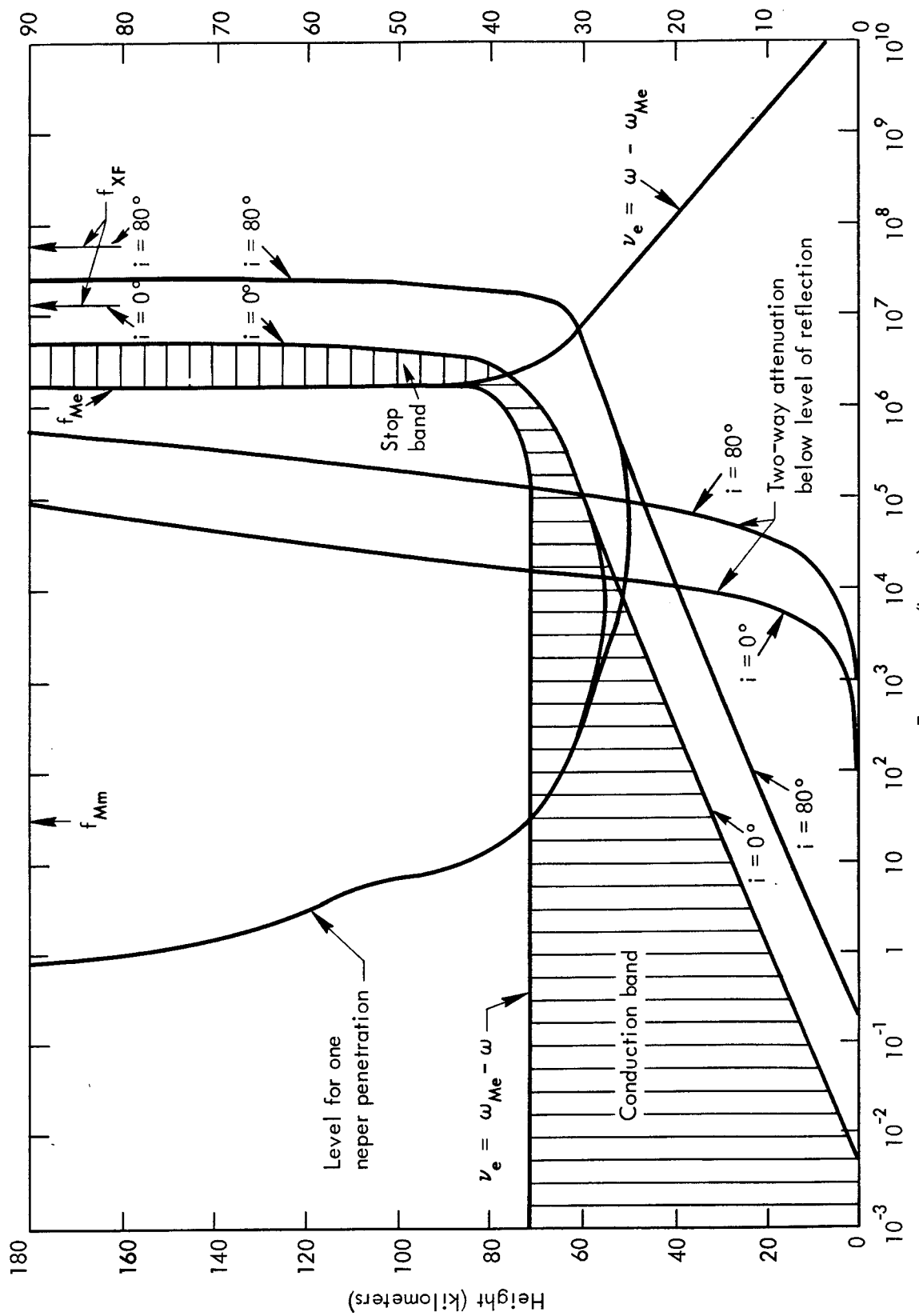

Fig. 10—Quasi-longitudinal propagation of the X wave for disturbed day conditions

are secondary, although they may still be responsible for some interesting attenuation.

Above the level where $\nu_i = \omega_{Mi}$ we see in Figs. 3 to 10 the familiar magneto-ionic behavior for quasi-longitudinal propagation in the absence of collisions. This involves a pass band below the ionic gyrofrequency for both the O and X waves (the hydromagnetic pass band), and, between the two gyrofrequencies, a stop band for the O wave and a pass band for the X wave (the whistler pass band). Above the usual critical frequency there is the electromagnetic pass band. In Figs. 3 to 10, pass bands are unstriped and stop bands are striped horizontally.

It will be noticed in Figs. 3 to 10 that the behavior above the level $\nu_i = \omega_{Mi}$ between the two gyrofrequencies extends below the ionic gyrofrequency in the altitude range between $\nu_i = \omega_{Mi}$ and $\nu_e = \omega_{Me}$. This is true for both the O and X waves. In Fig. 3 the whistler stop band for the O wave extends down through the hydromagnetic frequency band in the height range between $\nu_i = \omega_{Mi}$ and $\nu_e = \omega_{Me}$; whether or not this stop band below the ionic gyrofrequency is thick enough in relation to the wavelength in the medium to be effective as a stop band will be investigated later in this report. In Fig. 4 the whistler pass band for the X wave extends down through the hydromagnetic frequency band in the height range between $\nu_i = \omega_{Mi}$ and $\nu_e = \omega_{Me}$, thereby converting the entire region for which $\nu_e < \omega_{Me} - \omega$ into a single pass band for the X wave. Whistler behavior extends below the ionic gyrofrequency in the height interval between $\nu_i = \omega_{Mi}$ and $\nu_e = \omega_{Me}$ because, in these circumstances, collisions inhibit motion of the ions while permitting motion of the electrons. This is what happens for a different reason under normal whistler conditions, where it is the combined effect of inertia and the earth's magnetic field that inhibits ion and permits electron motion.

Besides pass bands and stop bands, there is shown at sufficiently low frequencies in each of Figs. 3 to 10 a conduction band indicated by vertical striping. This is the region where the square of the refractive index is dominated by its imaginary part, so that the refractive index has properties similar to those encountered in a metal. The thickness of the conduction band varies with frequency, and this

thickness has to be compared with the "skin depth" before we know whether the conduction band is mainly transparent or mainly reflecting at any particular frequency.

The pass, stop, and conduction bands in Figs. 3 to 10 for vertical propagation may be defined as the regions where the square of the refractive index is mainly real and positive (pass band), mainly real and negative (stop band), and mainly imaginary and negative (conduction band). Following Crain and Booker,[4] we may take the refractive index n as given by

$$n^2 = 1 - A - jB \tag{2}$$

where A and B are real,* and define boundaries for angle of incidence i as follows:

1. The boundary between a pass band and a stop band may be taken as

$$A = \cos^2 i \tag{3}$$

2. The boundary between a conduction band and a pass band may be taken as

$$B = \cos^2 i \tag{4}$$

3. The boundary between a stop band and a conduction band may be taken as

$$A = B \tag{5}$$

As shown by Field and Engel[9] a coefficient somewhat greater than unity on the right-hand side of Eq. (4) is desirable. Such a coefficient was in fact used in the calculations; the curves showing the

*See the Appendix for equations which express A and B in terms of ionospheric properties.

low-frequency boundary of the electromagnetic pass band then require slight smoothing where the phenomenon on the other side of the boundary changes from conduction-band behavior to stop-band behavior.

The low-frequency boundary of the electromagnetic pass band is given by Eq. (3) when $\nu_e < |\omega_{Me} \pm \omega|$ and by Eq. (4) when $\nu_e > |\omega_{Me} \pm \omega|$; therefore it depends on angle of incidence. The striped regions shown in Figs. 3 to 10 refer to vertical incidence (i = 0 deg). The extent to which these should be extended towards higher frequencies for glancing incidence is indicated by the almost parallel curve marked i = 80 deg.

At high frequencies the edge of the electromagnetic pass band shown in Figs. 3 to 10 is usually regarded as *the* height of reflection. In fact, of course, reflection takes place from a stratum extending above this height to a level conveniently defined as the level where the storage field has dropped to about 1 neper below the value at *the* height of reflection. Using the WKB approximation, this level for 1 neper penetration has been calculated and plotted in Figs. 3 to 10.

In Fig. 3, the reflecting stratum acquires more than "pencil thickness" below about 10^5 Hz for vertical incidence and 10^6 Hz for glancing incidence. The curve for 1 neper penetration intersects the top of the stop band just below the ionic gyrofrequency. At all lower frequencies the combined stop and conduction band for the O wave has a thickness less than the "skin depth" as understood for a metal. Below about 10 Hz in Fig. 3, therefore, the conduction and stop bands are in fact transparent.

The frequency at which the curve for 1 neper penetration intersects the top of the stop band for the O wave (Figs. 3, 5, 7, 9) may be defined as the hydromagnetic, or inferior, penetration frequency of the ionosphere for the O wave. A similar inferior penetration frequency of the ionosphere can be defined for the X wave by the intersection of the curve for 1 neper penetration with the top of the conduction band (Figs. 6 and 10). In the case of Fig. 4 the attenuation in the conduction band at vertical incidence is less than 1 neper, so that the conduction band is to be classified as transparent; it acts like a metal film whose thickness is small compared with the skin depth. The interpretation of Fig. 8 requires care and is discussed later.

Between the inferior penetration frequency of the ionosphere just discussed and the usual, or superior, penetration frequency known as the critical frequency, the ionosphere reflects*. Nevertheless the attenuation of the reflected wave below the level of reflection may be quite substantial. This attenuation is therefore shown in Figs. 3 to 10, using the right-hand vertical scale.

The attenuation below the level of reflection in Figs. 3 to 10 has been calculated by the methods developed by Booker and Crain[10] and by Booker, Fejer, and Lee.[11] In view of the criticism by von Roos[12] of the theorem given by Booker, Fejer, and Lee,[11] it should perhaps be emphasized that the theorem does in fact apply with adequate accuracy at all levels in Figs. 3 to 10 below the curves corresponding to Eq. (1). Von Roos is quite correct in stating that the theorem is unsatisfactory when the effect of the earth's magnetic field is vital. Thus, it is unsatisfactory for calculating the attenuation of the reflected O wave in the VHF band under ambient night conditions (Fig. 3); however, the attenuation is then relatively small.

Figures 3 to 10 show superior penetration frequencies (critical frequencies) for the ionosphere that depend on maximum electron density and angle of incidence (based on a plane earth and ionosphere) in the usual way. On the other hand, they also indicate inferior penetration frequencies for the ionosphere arising from thinness of the reflecting stratum as listed in Table 1.

Of course, the inferior penetration frequency of the ionosphere is not as precise a concept as the superior penetration frequency. In the neighborhood of the inferior penetration frequency there is an interval of about an octave over which significant partial reflection and penetration is taking place. However, there is a sense in which the inferior penetration frequency tends to be more precise than the superior penetration frequency. The inferior penetration frequency shows little dependence on angle of incidence because, at the inferior penetration

*This reflection occurs within the context of the WKB treatment used here. As discussed earlier, a full-wave treatment would indicate significant gradient reflection at frequencies of 100 Hz or less.

Table 1

INFERIOR PENETRATION FREQUENCY OF THE IONOSPHERE IN HERTZ
(QUASI-LONGITUDINAL PROPAGATION)

Condition	O Wave		X Wave	
	i = 0°	i = 80°	i = 0°	i = 80°
Ambient night	f_{Mi}	f_{Mi}	f_{Me}	f_{Me}
Disturbed night	0.6	0.6	200	300
Ambient day	1.6	1.6	10^4	10^4
Disturbed day	0.4	0.4	25	25

frequency, the refractive index in the ionosphere is usually high, so that waves incident at almost any angle in free space are refracted to nearly vertical propagation in the ionosphere. The inferior penetration frequencies shown in Table 1 are reasonably close to the maximum frequencies of the lower ionospheric transmission bands defined on the basis of a different criterion in Ref. 1.

Table 1 shows that under ambient night conditions, the inferior penetration frequency is given essentially by the ionic gyrofrequency for the O wave and by the electronic gyrofrequency for the X wave. Collisions are relatively unimportant at any level where appreciable ionization exists under ambient night conditions.

The same would appear to be true at first sight for the X wave under ambient day conditions (Fig. 8). However, this is somewhat deceiving. For vertical incidence the conduction band shown by vertical striping in Fig. 8 is practically transparent, so that no major reflection of the X wave occurs for vertical incidence below the electronic gyrofrequency. Nevertheless, the total attenuation of the transmitted X wave is significant except well down in the hydromagnetic band, and it becomes prohibitive above about 10^4 Hz. Thus it is more appropriate in Table 1 to list the inferior penetration frequency for the X wave at vertical incidence under ambient day conditions as about 10^4 Hz.

Moreover, for the X wave under ambient day conditions, glancing incidence differs from vertical incidence in a rather significant way.

For glancing incidence (i = 80 deg) the curve for 1 neper attenuation in Fig. 8 intersects the top of the conduction band at 10^4 Hz and again at 2.5×10^6 Hz. Between these two frequencies reflection of the X wave at glancing incidence would therefore take place from the conduction band under ambient day conditions. It should be noted from the right-hand scale, however, that attenuation below the level of reflection is prohibitively high above about 10^5 Hz.

For the O wave under ambient day conditions (Fig. 7) the inferior penetration frequency of the ionosphere occurs where the wavelength is long enough to make the combined conduction and stop bands less than a "skin depth" in thickness. This occurs at about 1.6 Hz for all angles of incidence. Even major disturbance of the D region of the ionosphere (Fig. 9) only drops this to 0.4 Hz.

At night major disturbance of the D region drops the inferior penetration frequency of the ionosphere for the O wave from roughly the ionic gyrofrequency to 0.6 Hz, a value intermediate between 1.6 Hz for ambient day conditions and 0.4 Hz for disturbed day conditions (Table 1). Thus, for disturbed night conditions, as well as for day conditions (ambient or disturbed), the inferior penetration frequency of the ionosphere for the O wave is in the general vicinity of 1 Hz. It is only under undisturbed night conditions that it rises towards the ionic gyrofrequency for molecules (around 30 Hz).

The inferior penetration frequency of the ionosphere for the X wave is much more dependent upon the degree of disturbance. Whereas for ambient night conditions the inferior penetration frequency of the ionosphere for the X wave is not much less than the electronic gyrofrequency, it drops to a few hundred hertz under disturbed night conditions. It drops to a few tens of hertz under disturbed day conditions from an ambient day value of about 10^4 as discussed above.

Curves showing the overall attenuation for transmission through the ionosphere to a high satellite using the ionospheric models under discussion are given elsewhere.[1] The same report presents curves for the variation of the rate of attenuation with height for numerous frequencies from 1 Hz to 100 kHz. A feature of these curves at frequencies below about 100 Hz is that they show, in addition to the usual

electronic behavior, maxima of attenuation in the vicinity of the level where $\nu_i = \omega_{Mi}$ (between 110 and 120 km) arising from ionic collisions with neutral molecules. These maxima are of particular interest in the neighborhood of the ionic gyrofrequency. This is the cause of the dip in the curve for 1 neper penetration near the ionic gyrofrequency in Fig. 8 and for the kink in the same curve in Fig. 10. Another interesting feature of the results in Ref. 1 is that under ambient conditions there is actually a local maximum in the transmission loss of the X wave through the ionosphere near the ionic gyrofrequency of the order of 2 dB by night and 11 dB by day, virtually independent of angle of incidence. Under disturbed conditions, however, this local maximum becomes an almost insignificant ledge on a rapid rise of transmission loss with frequency near the ionic gyrofrequency.

APPENDIX

In this Appendix we list the parameters and equations used to obtain the numerical results given in this report and in Ref. 1. The equations are the well known ones of the magneto-ionic theory including positive and negative ions and are stated without derivation. A discussion of the range of applicability of the equations is given in Section II. We begin by listing parameters and defining symbols and then give the equations:

N_e = electron density, m^{-3}
N_{ia-} = density of negatively charged atoms, m^{-3}
N_{im-} = density of negatively charged molecules, m^{-3}
N_{ia+} = density of positively charged atoms, m^{-3}
N_{im+} = density of positively charged molecules, m^{-3}
Θ = temperature, °K

The various charged-particle density profiles were used to obtain Fig. 1. The ions were assumed molecular below 150 km and atomic above 160 km; Θ was obtained from Ref. (13); $Z = \rho/1.225$, where ρ is neutral atmospheric density in kg m^{-3} and was taken from Ref. 3. The electron-neutral and ion-neutral collision frequencies ν_e and ν_i were obtained from the simple approximate relations

$$\nu_e = 6.1 \times 10^{-9} \left(\frac{\Theta}{300}\right)^{-3/2} N_i + 1.8 \times 10^{11} Z \quad \text{sec}^{-1}$$

$$\nu_i = 4 \times 10^{9} Z \quad \text{sec}^{-1}$$

Constants which were used are

$a = 6370$ km
$e = 1.602 \times 10^{-19}$ C
$m_e = 9.106 \times 10^{-31}$ kg
$m_a = 16 \times 1837 \times m_e$
$m_m = 29 \times 1837 \times m_e$
$c = 2.998 \times 10^{8}$ m/sec
$\epsilon_o = 8.854 \times 10^{-12}$ F/m

The squares of the various angular plasma frequencies (in hertz) are given by

$$\omega_{Ne}^2 = \frac{e^2}{\varepsilon_o m_e} N_e$$

$$\omega_{Na-}^2 = \frac{e^2}{\varepsilon_o m_a} N_{ia-}$$

$$\omega_{Nm-}^2 = \frac{e^2}{\varepsilon_o m_m} N_{im-}$$

$$\omega_{Na+}^2 = \frac{e^2}{\varepsilon_o m_a} N_{ia+}$$

$$\omega_{Nm+}^2 = \frac{e^2}{\varepsilon_o m_m} N_{im+}$$

and the angular gyrofrequencies by

$$\omega_{Me} = 2\pi \times 1.7 \times 10^6 (1 - 3\frac{z}{a})$$

$$\omega_{Ma} = \frac{1}{16 \times 1837} \omega_{Me}$$

$$\omega_{Mm} = \frac{1}{29 \times 1837} \omega_{Me}$$

$$\omega = 2\pi f$$

where Z is the height above the ground in kilometers and f is the wave frequency in hertz.

We now list the following functions, where the upper sign corresponds to the O wave and the lower sign to the X wave.

$$A_e = \frac{\omega_{Ne}^2 \, (\omega \pm \omega_{Me})}{\omega[(\omega \pm \omega_{Me})^2 + \nu_e^2]}$$

$$A_{a-} = \frac{\omega_{Na-}^2 \, (\omega \pm \omega_{Ma})}{\omega[(\omega \pm \omega_{Ma})^2 + \nu_i^2]}$$

$$A_{m-} = \frac{\omega_{Nm-}^2 \, (\omega \pm \omega_{Mm})}{\omega[(\omega \pm \omega_{Mm})^2 + \nu_i^2]}$$

$$A_{a+} = \frac{\omega_{Na+}^2 \, (\omega \mp \omega_{Ma})}{\omega[(\omega \mp \omega_{Ma})^2 + \nu_i^2]}$$

$$A_{m+} = \frac{\omega_{Nm+}^2 \, (\omega \mp \omega_{Mm})}{\omega[(\omega \mp \omega_{Mm})^2 + \nu_i^2]}$$

$$B_e = \frac{\omega_{Ne}^2 \, \nu_e}{\omega[(\omega \pm \omega_{Me})^2 + \nu_e^2]}$$

$$B_{a-} = \frac{\omega_{Na-}^2 \, \nu_i}{\omega[(\omega \pm \omega_{Ma})^2 + \nu_i^2]}$$

$$B_{m-} = \frac{\omega_{Nm-}^2 \, \nu_i}{\omega[(\omega \pm \omega_{Mm})^2 + \nu_i^2]}$$

$$B_{a+} = \frac{\omega_{Na+}^2 \, \nu_i}{\omega[(\omega \mp \omega_{Ma})^2 + \nu_i^2]}$$

$$B_{m+} = \frac{\omega_{Nm+}^2 \, \nu_i}{\omega[(\omega \mp \omega_{Mm})^2 + \nu_i^2]}$$

$$A = A_e + A_{a-} + A_{m-} + A_{a+} + A_{m+}$$

$$B = B_e + B_{a-} + B_{m-} + B_{a+} + B_{m+}$$

The refractive index is given by

$$n = (1 - A - jB)^{1/2} \qquad R(n) > 0,\ I(n) < 0$$

where $j = \sqrt{-1}$, whence the local wavelength can be computed from

$$\lambda = \frac{c}{f} \frac{1}{R(n)} \times 10^{-3} \quad \text{km}$$

By defining

$$q = (\cos^2 i - A - jB)^{1/2} \qquad R(q) > 0,\ I(q) < 0$$

and

$$\alpha_T = 8.686 \frac{\omega}{c} I(q) \times 10^3 \quad \text{dB/km}$$

the transmission loss is computed from

$$T = \int_0^z \alpha_T dz \quad \text{dB}$$

After defining

$$\alpha_R = 8.686 \frac{\omega}{c} B \sec i \times 10^3 \quad \text{dB/km}$$

the reflection loss was computed from

$$R = \int_0^z \alpha_R \, dz \quad \text{dB}$$

REFERENCES

1. Booker, H. G., C. M. Crain, and E. C. Field, *Transmission of Electromagnetic Waves Through Normal and Disturbed Ionosphere,* The Rand Corporation, R-558-PR, November 1970.

2. Ginzburg, V. L., *Propagation of Electromagnetic Waves in Plasma,* Gordon and Breach Science Publishers, New York, 1961.

3. Crain, C. M., *A Note on Persisting Radio Propagation Effects After High-Altitude Nuclear Bursts,* The Rand Corporation, RM-4037-PR, March 1964; also published in *J. Geophys. Res.,* Vol. 69, No. 21, November 1, 1964, pp. 4717-4721.

4. Crain, C. M., and H. G. Booker, *The Effect of Ions on Low Frequency and Very Low Frequency Propagation in an Abnormally Ionized Atmosphere,* The Rand Corporation, RM-4031-PR, February 1964; also published in *J. Geophys. Res.,* Vol. 69, No. 21, November 1, 1964, pp. 4713-4716.

5. Knapp, W. S., and P. G. Fischer, *Aids in the Study of Electromagnetic Blackout,* DASA Report 70 TMP 12, General Electric Company, July 1970.

6. Field, E. C., and C. Greifinger, *The Transmission of Geomagnetic Micropulsations Through the Ionosphere and Lower Exosphere,* The Rand Corporation, RM-4494-ARPA, April 1965; also published in *J. Geophys. Res.,* Vol. 70, No. 19, October 1, 1965, pp. 4885-4899.

7. Jones, R. M., "Ray Theory for Lossy Media," *Radio Science,* Vol. 5, No. 5, May 1970, p. 793.

8. Booker, H. G., and R. B. Dyce, "Dispersion of Waves in a Cold Magnetoplasma from Hydromagnetic to Whistler Frequencies," *Radio Science Journal of Research NBS/USNC-URSI,* Vol. 69D, No. 4, April 1965, p. 463.

9. Field, E. C., and R. D. Engel, "The Detection of Daytime Nuclear Bursts Below 150 km by Prompt VLF Phase Anomalies," *Proc. IEEE,* Vol. 53, No. 12, December 1965, pp. 2009-2017.

10. Booker, H. G., and C. M. Crain, *LF and VLF Reflection Loss in the Lower Ionosphere: A Theorem on Absorption and Its Application,* The Rand Corporation, RM-5249-PR, March 1967.

11. Booker, H. G., J. A. Fejer, and K. F. Lee, "A Theorem Concerning Reflection from a Plane Stratified Medium," *Radio Science* (new series), Vol. 3, No. 3, March 1968, pp. 207-213.

12. Van Roos, O., "A Note on the Applicability of the Booker Theorem to Magnetoactive Plasmas," *Radio Science* (new series), Vol. 5, No. 5, April 1970, pp. 693-695.

13. Minzer, R. A., K.S.W. Champion, and H. L. Pond, *The ARDC Model Atmosphere, 1959,* Air Force Cambridge Research Center, TR-59-267, August 1959.